Melting Thresholds of Materials Irradiated with a Wide Class of Pulsed Electron Beams

Alexey Markov *

Posted Date: 14 July 2023

doi: 10.20944/preprints202307.0970.v1

Keywords: pulsed electron beam; melting threshold; pulsed heating; refractoriness series of metals

Article

Melting Thresholds of Materials Irradiated with a wide Class of Pulsed Electron Beams

Alexey B. Markov *

Tomsk Scientific Center SB RAS, Russia, 634055, Tomsk, 10/4 Akademicheskii Prospect
* Correspondence: a.markov@hq.tsc.ru; Tel.: +73822491173

Abstract: Based on the prosed criterion of the type of heating, a classification of the sources of pulsed electron beams was carried out, for better understanding both the nature of the thermal processes occurring under irradiation and for predicting their suitability for certain applications. The melting thresholds of materials were calculated over the wide ranges of accelerating voltages and pulse durations. On the basis of calculations, a refractoriness series of metals for surface-volume pulsed heating was proposed.

Keywords: pulsed electron beam; melting threshold; pulsed heating; refractoriness series of metals

1. Introduction

Recently, sources of pulsed electron beams (PEBs) have been widely used as a tool for delivering of energy in order to initiate desirable physicochemical processes in irradiated targets [1–33]. As a rule, energy is delivered to the surface layer of the target, the thickness of which can vary from fractions to hundreds of micrometers. According to the reported data, there is a fairly great variety of PEBs types that have been designed for various purposes, such as homogenizing surface layers of metallic materials via their re-melting, forming surface alloys, generating microwave or X-ray radiation, sterilizing medical materials, processing plant seeds, etc. Table 1 presents the names of some existing PEB source and their key parameters, namely U accelerating voltages and τ pulse durations. In addition, their beam factors (BFs) are also highlighted, the physical meaning of which is discussed below in the 'Results' section.

Table 1. The key parameters of some sources of PEBs.

Name	Accelerating voltage U, kV	Pulse duration τ, μs	Beam factor, kg/(m²s$^{1/2}$)	Refs.
SOLO	5–25	50–200	0.1–1.8	1-5
RITM	5–25	2.5	0.7–7.9	6-20
GESA-I	50–150	4–40	5.6–91.9	21-22
DUET	100–200	10–300	5.8–89.4	23-25
GESA-II	200–400	5–250	17.9–357.8	21-22
TEU-500	400	0.1	2529	26-28
SINUS-7	1000	0.05	14142	29-32

As follows from the presented data, the U accelerating voltages vary from 5 up to 1000 kV, i.e., the minimum and maximum values differ by 200 times, while the τ pulse durations evolve from 0.05 up to 300 μs, i.e., by a factor of 6000. Undoubtedly, such sources of PEBs initiate thermal processes in targets that differ in parameters and dynamics; therefore, the classifying both PEBs and the initiated thermal processes is required. For this purpose, simple criteria are generally used: beams can be classified as continuous or pulsed, relativistic or non-relativistic, high- or low-current. All these criteria depend exclusively on the beam parameters and are independent of the target material type. It is interesting to consider more complex benchmarks that would make it possible to understand the

Preprints (www.preprints.org) | NOT PEER-REVIEWED | Posted: 14 July 2023 doi:10.20944/preprints202307.0970.v1

nature of processes occurring under irradiation of a particular target and the possibility of using a beam for certain applications. Naturally, such criteria should depend not only on the beam parameters, but also on the target materials. The first aim of this research has been to classify PEBs and briefly analyze the thermophysical processes occurring in a target based on one of these thermophysical criterion, which is called the *heating type criterion*. It depends on the parameters of both the beam and the target, and its definition will be given below in *Theoretical background* section.

In processing of metallic materials with PEBs, the initial melting mode is one of the well-known and widely applied for a number of practical purposes, such as surface smoothing or detecting of contaminants on the irradiated surface [16,19]. In this case, the first portions of the melt appear on the target surface. The mode of initial melting for a particular material is determined by the parameters of PEBs. However, the specific energy (power) absorbed by the target in the mode of initial melting, called the material melting threshold (MMT), is already a characteristic of the substance. Among other things, the MMT can be used as a kind of *reference point* for a comparative analysis of the effects of different PEBs on the same material. Respectively, the second research aim has been to analyze the temperature modes induced by PEBs in a wide range of their parameters, judging by the achievement of the MMT level.

2. Materials and Methods

In this research, the $\boldsymbol{L_{tm}}$ MMT is understood as the power density of PEBs [W/m^2] at which the melting temperature is reached on the target surface by the end of a pulse. Also, the energy MMT (EMMT) concept [J/m^2] is applied, which is related to MMT as

$$\boldsymbol{E_{tm} = L_{tm}\tau}. \quad (1)$$

Computer simulation of the dynamics of temperature fields under irradiation with PEBs has been carried out using the 'HEATPACK-1.0' software package, described in [34,35]. In this case, a one-dimensional non-stationary heat equation has been solved numerically with a mixed surface and volume heat sources, considering the energy loss of an electron beam in an irradiated target. The initial temperature of the target was assumed to be room temperature. The target rear side has been supposed to be thermally insulated. The melting process has been simulated by the effective specific heat method. However, in this study, the parameters of PEBs have been chosen so that the target surface temperature reached the melting point by the end of a pulse and does not exceed it.

In computer simulation, rectangular-shaped pulses have been considered, during the pulse duration τ at constant both $U(t)$ accelerating voltage and $j(t)$ current density. The U accelerating voltages have been varied in a wide range from 10^3 up to 10^6 V when studying the MMT.

Numerous materials have been considered as targets, the list of which is given in Table 2 with their key thermophysical properties [36]. In addition, their materials factors (MFs) are presented, the physical meaning of which is discussed below in the *Results* section. The BaseM material is a virtual pseudo-metal that does not exist in nature. Its properties are collective and close to some average values of a wide class of real metals and alloys. Its MMT and EMMT values have been used as measuring units, against which those of other materials have been calculated to facilitate comparison.

Table 2. The key thermophysical properties of the investigated metals.

Metal	Density ρ, kg/m^3	Heat capacity c_p, J/(kg K)	Thermal conductivity λ, W/(m K)	Melting point T_m, K	Material factor, kg/(m^{2}s$^{1/2}$)
Mg	$1.70{\cdot}10^3$	1037	156	923	32.0
Be	$1.85{\cdot}10^3$	1825	201	1551	28.5
Al	$2.70{\cdot}10^3$	900	237	933	53.3
Ti	$4.54{\cdot}10^3$	522	22	1943	27.6
BaseM	$7.00{\cdot}10^3$	560	67	1000	57.9
Cr	$7.20{\cdot}10^3$	448	94	2130	77.7
Fe	$7.90{\cdot}10^3$	448	80	1812	75.1

Preprints (www.preprints.org) | NOT PEER-REVIEWED | Posted: 14 July 2023 doi:10.20944/preprints202307.0970.v1

Ni	$8.90 \cdot 10^3$	445	91	1453	85.3
Cu	$8.92 \cdot 10^3$	384	400	1357	192.8
Zr	$6.51 \cdot 10^3$	277.7	22.7	2155	46.1
Mo	$1.02 \cdot 10^3$	250	138	2893	150.2
Ag	$1.05 \cdot 10^3$	235	429	1235	276.9
W	$1.93 \cdot 10^3$	132	163	3695	308.2

3. Theoretical Background

Assuming that the surface layer of an irradiated target consists of a set of successively arranged parallel microscopic plates, the overall target area can be heated during a pulse duration τ in two ways: sequentially (1) or simultaneously (2). Sequential (plate-by-plate) heating (1) is caused by thermal conduction, when the heating front propagates at a certain speed from the surface into the target. Simultaneous heating (2) of many microscopic plates occurs as a result of the instantaneous energy input into their integral area. According to solid state physics, any such a plate is a local subsystem of nuclei located in an electron gas. Respectively, it can receive energy (be heated) either from nuclear subsystems of neighboring plates, which corresponds to sequential heating or through the excited electron shell of an atom upon instantaneous heating. It should be noted that both heating modes are not associated with mass transfer.

As mentioned above, mathematically, the difference between the two heating modes lies in the fact that energy (heat) propagates with a certain finite speed, sequentially heating layer by layer in the first case, but a target is heated almost instantly in its entire volume in the second case, i.e., the energy propagation speed can be considered as infinite. So, the beam energy is completely released on the surface in the first case, and the r thickness of the energy release layer is zero. In the second case, it is above zero, corresponding to the extrapolated particle range in the target. So, it is heated with a surface source in the first case, but with a volume one otherwise. It is clear that surface heating, when the extrapolated particle range in the target r is zero, is a mathematical approximation, but in reality, energy is always released in a layer of finite thickness. However, if the thickness of the layer heated during a pulse via thermal conduction r_{th} is much greater than the r extrapolated particle range in the target, then the heating source can be considered as a surface one. On the contrary, if it is much thinner, then the heating source is a volume one. Let's introduce the γheating type criterion as follows

$$\gamma = \frac{r}{r_{th}}. \tag{2}$$

The γheating type criterion enables to understand the nature of thermal processes occurring in a target of a particular material under irradiation with PEBs.

Obviously, the following three options are possible:

$$\begin{cases} \gamma \gg 1, & \text{volume heating} \\ \gamma \sim 1 & \text{mixed heating} \\ \gamma \ll 1, & \text{surface heating} \end{cases} \tag{3}$$

For the general notation of the heat equation, two p_h and p_v auxiliary parameters have been added, which are equal to 0 for both $\gamma \gg 1$ and $\gamma \ll 1$ conditions, but are equal to 1 in all other cases.

It is known that a one-dimensional problem should be solved for calculating the $T(\vec{r},t)$ temperature at a point in a sample with a $\vec{r}$ radius vector at a t time if the following condition is fulfilled:

$$D/2 \gg r + r_{th}, \tag{4}$$

where D is the cross-sectional dimension of the homogeneous energy release region of an electron beam.

For most PEBs, the D parameter can be considered as their diameters. Condition (4) means that the beam radius should be much larger than a size of the heated near-surface region during the observation of the process. If the beam diameter is greater than sizes of the irradiated target, then this

Preprints (www.preprints.org) | NOT PEER-REVIEWED | Posted: 14 July 2023 doi:10.20944/preprints202307.0970.v1

condition is satisfied for any t values. In this case, temperature fields in targets irradiated with PEBs upto initial melting modes can be calculated by solving the one-dimensional non-stationary heat equation

$$\rho C(T)\frac{\partial T(x,t)}{\partial t} = \frac{\partial}{\partial x}\left(\lambda(T)\frac{\partial T(x,t)}{\partial x}\right)p_h + L_V(x,t)p_v, \quad x \in [0;l], \qquad t \in [0;\tau) \tag{5}$$

with both initial and boundary conditions, the left of which has the form

$$-\lambda(T)\frac{\partial T}{\partial x}\Big|_{x=0} = L_s(t)p_h, \tag{6}$$

where $L_V(x,t)$ is the heat source function or the volume heat source, $L_s(t)$ is the surface heat source.

In the heat equation, the use of the p_h and p_v auxiliary parameters enables to simplify calculations when considering edge cases. If $\gamma \gg 1$, i.e., heating is performed by a volume heat source, then $p_h = 0$ and the first term on the right side of equation (5), as well as the right side of the boundary condition (6) are equal to zero. If $\gamma \ll 1$ due to the application of a surface heat source, then then $p_v = 0$ and the second term on the right side of equation (5) vanishes. In all other cases, the surface is heated with both $L_V(x,t)$ and $L_s(t)$ heat sources during a pulse duration.

It should be clarified that the power density is understood to be that already absorbed by a target, but not emitted by an electron beam. It is clear, only part of the electron beam energy is absorbed under real conditions, while the rest one (up to 40%) is reflected.

3.1. Heating with a Volume Heat Source

Let us consider the $\gamma \gg 1$ case in more detail, when equation (5) is transformed into the following one

$$\rho c(T)\frac{\partial T(x,t)}{\partial t} = L_V(x,t), \tag{7}$$

which is integrated easy

$$T(x,t) = \int_0^t \frac{L_V(x,t)}{\rho c(T)}dt + T_0(x), \tag{8}$$

where

$$L_V(x,t) = \frac{j(t)U(t)}{r(t)} f\left(\frac{x}{r},t\right). \tag{9}$$

In this case, $f\left(\frac{x}{r},t\right)$ is the electron energy loss function normalized by its extrapolated range (depth of penetration).

Considering that

$$r(t) = C_0(U(t))^{3/2} / \rho, \tag{10}$$

where C_0 = $10^{-17/2}$ kg/(m^{2}W$^{3/2}$) and ρ is the density of the target material [34]. Substituting the $r(t)$ expression in formula (9), it can be written as

$$L_V(x,t) = \frac{j(t)\rho}{C_0 U(t)^{1/2}} f\left(\frac{x}{r},t\right), \tag{11}$$

and, combining equations (11) and (8), finally it corresponds to

$$T(x,t) = \frac{1}{C_0}\int_0^t \frac{j(t)f(\frac{x}{r},t)}{U^{\frac{1}{2}}(t)C(T)}dt + T_0(x). \tag{12}$$

Taking accelerating voltage $U(t) = const$ and the material specific heat capacity $C(T) = const$ in expression (12), it has been rewritten as

Preprints (www.preprints.org) | NOT PEER-REVIEWED | Posted: 14 July 2023 doi:10.20944/preprints202307.0970.v1

$$T(x,t) = \frac{f(\frac{x}{r})}{C_0 U^{\frac{1}{2}} C} \int_0^t j(t)\, dt + T_0(x). \quad (13)$$

It can be concluded from the last expression (13) that temperature is proportional to the area under the j current density profile and does not depend on its shape. Assuming $j(t) = const$ and considering the surface temperature by the end of a pulse ($t = \tau$), it can be stated that

$$T(0,\tau) = \frac{f(0) j \tau}{C_0 U^{\frac{1}{2}} C} + T_0(x). \quad (14)$$

As follows from expressions (13) and (14), temperature variations in the surface layer are directly proportional to j current density, and inversely proportional to the square root of U accelerating voltages. Also, temperature is inversely proportional to the specific heat of the target material and does not depend on its thermal conductivity. The surprise in these formulas is that temperature does not depend on the material density, although the thickness of the energy release layer is varied for different densities of the target material. The reason is the fact that the number of nuclei of a substance, to which the beam energy is transferred, remains unchanged upon varying its density. On the one hand, the specific density of nuclei increases in direct proportion to the substance density, and temperature should decrease. On the other hand, the energy release volume reduces due to the inverse relationship between the electron range and the substance density. Thus, these two opposite tendencies compensate each other, and temperature does not change, but the heated surface layer thickness varies in proportion to the substance density.

Equating $T(0,\tau) = T_m$ in expression (14) and making some transformations, it turns to be

$$L_{tm1} = j_{m1} U = [C(T_m - T_0)] \frac{C_0}{f(0)} \frac{U^{\frac{3}{2}}}{\tau}. \quad (15)$$

Expression (15) determines the threshold of the absorbed electron beam power density at which the melting temperature is reached on the target surface, in other words, this expression specifies the MMT in the volume heating case (at $\gamma \gg 1$).

3.2. Heating with a Surface Heat Source

In the $\gamma \ll 1$ case, equation (5) is transformed into (16) with the left boundary condition (17)

$$\rho c(T) \frac{\partial T(x,t)}{\partial t} = \frac{\partial}{\partial x}\left(\lambda(T) \frac{\partial T(x,t)}{\partial x}\right), \quad (16)$$

$$-\lambda(T) \frac{\partial T}{\partial x}\Big|_{x=0} = L_s(t). \quad (17)$$

If $L_s(t)=const$, then the solution of equation (16) with the boundary condition (17) has the following form [37]:

$$T(x,t) = \frac{2L_s\sqrt{at}}{\lambda} ierfc\left(\frac{x}{2\sqrt{at}}\right) + T_0(x). \quad (18)$$

Describing the a thermal diffusivity in accordance with its definition and considering temperature on the target surface by the end of a pulse, the following dependence can be written:

$$T(0,\tau) = 2L_s \sqrt{\frac{\tau}{\rho c \lambda}} ierfc(0) + T_0(x). \quad (19)$$

Equating $T(0,\tau) = T_m$ in expression (19) and making some transformations, it turns to be

$$L_{tm2} = j_{m2} U = \left[\sqrt{\rho c \lambda}(T_m - T_0)\right]\left(2 ierfc(0)\sqrt{\tau}\right)^{-1}. \quad (20)$$

Preprints (www.preprints.org) | NOT PEER-REVIEWED | Posted: 14 July 2023 doi:10.20944/preprints202307.0970.v1

Expression (20) determines the threshold of the absorbed electron beam power density at which the melting temperature is reached on the target surface, in other words, this expression specifies the MMT in the surface heating case (at $\gamma \ll 1$).

It can be concluded from expression (20), that L_{tm2} values depend as a power function with a degree of ½ not only on thermal conductivity, but also on other thermophysical properties of the target material, such as density and heat capacity. In addition, the melting temperature has the greatest influence on the MMT according to the directly proportional relationship. From general considerations, it is clear that the PPM should decrease with increasing pulse duration. It can be seen from the formula that this is the case, the PPM falls as the root of the pulse duration. So, its rising by 100 times lowers MMT by 10 times.

4. Results

Let us find an expression for the γheating type criterion in a case of target irradiation with PEBs. Firstly, an r_{th}thickness should be assessed for the layer heated via thermal conduction during a τ pulse duration. It can be written based on the $\Delta T(0,\tau) \gg \Delta T(r_{th},\tau)$ condition and taking into account the temperature field expression (18):

$$r_{th} = 2\sqrt{a\tau}. \tag{21}$$

Then, substituting formulas (21) and (10) into (2), the following dependence of the γ heating type criterion can be obtained:

$$\gamma = C_0 \left(\frac{U^{3/2}}{\tau^{1/2}}\right) / \left(\frac{4\lambda\rho}{c_p}\right)^{1/2}. \tag{22}$$

It follows from expression (22) the that γ values are positive in all cases. If the target material is irradiated with different types of PEBs, the γ values are the same if the $U^3/\tau = const$ condition is met. Thus, a τpulse duration has to be increased by 8 times when a U accelerating voltage is doubled.

It should be noted that the dividend on the right side of expression (22) depends solely on the parameters of PEBs, while the divisor only on the material properties (the mentioned above BF and MF parameters, respectively). The calculated BF ranges for sources of PEBs are given in the fourth column of Table 1, and the MF for the studied metals are presented in the last column of Table 2. If BF is numerically equal to MF, then γ=1, which means that contributions from the volume and surface sources are equal, i.e., the heating type is volume-surface or mixed. Accordingly, if the dividend is much larger or smaller than the divisor, then the heating type is volume or surface, respectively.

Thereby, in accordance with conditions (3) and formula (22), the 'BF–MF' phase space can be divided into three Z1–Z3 regions, which correspond to the volume, mixed and surface heating types, respectively. All of them are highlighted in different colors in Figure 1. In the Z2 central region, there is a dotted line corresponding to the γ heating type criterion of 1. In addition, dashed lines are plotted in Figure 1, limiting the range of BF changes for each of the sources of PEBs given in Table 1. The dashed lines should extend over the entire MF range, but they are limited to small segments in order not to clutter the drawing. Between the dashed lines limiting each BF range, the corresponding PEB source name is given.

It follows from Figure 1 that the sources of PEBs fall into different Z1–Z3 phase space regions, while, depending on its parameters and types of the target, the same PEB can be located in several areas. So, the 'RITM' and 'SOLO' facilities are in the Z3 region, i.e., their heating sources are of the surface type for almost all target materials. However, part of the dotted line of the upper 'RITM' range is in the mixed heating region. This means that the heating source is of the mixed type for the Ti, Mg and Al targets at U accelerating voltages at the upper level of the range. The 'GESA' and 'DUET' sources of PEBs are in the Z2 mixed heating region. Nevertheless, both 'GESA-1' and 'DUET' sources can be considered of the surface type in the lower energy range at high τpulse durations for most target materials, except for Ti and Mg. The 'TEU-500' and 'SINUS-7' ones fall into the Z1 volume heating region, but 'TEU-500' is in the region of mixed heating when irradiating W.

Preprints (www.preprints.org) | NOT PEER-REVIEWED | Posted: 14 July 2023 doi:10.20944/preprints202307.0970.v1

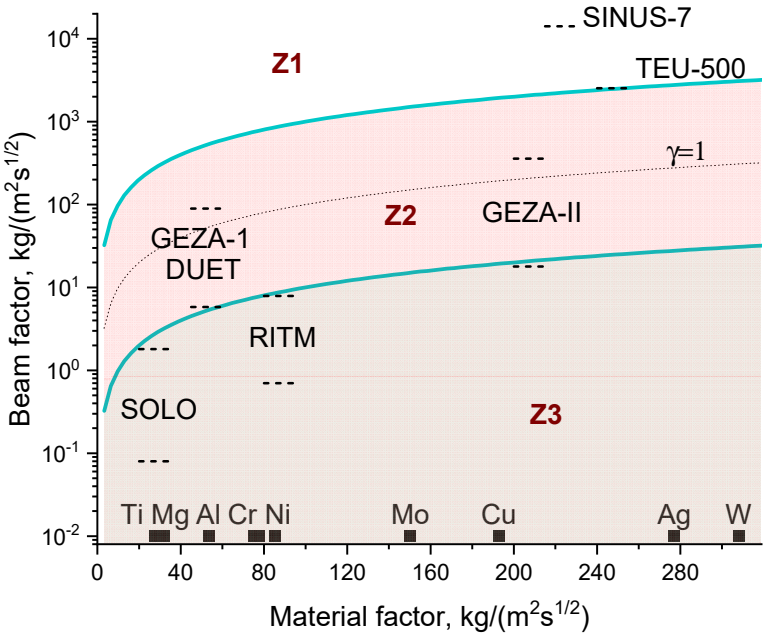

Figure 1. The sources of PEBs in the 'BF–MF' phase space. The Z1–Z3 regions correspond to volume, mixed and surface heating, respectively.

The L_{tm1} and L_{tm2} values, given by formulas (15) and (20) for the $\gamma \gg 1$ and $\gamma \ll 1$ cases, respectively, depend both on the material thermophysical properties and on the parameters of PEBs. It has been of interest to calculate the contribution of the material thermophysical properties to MMT, i.e., parts of the formulas in square brackets. The obtained results are shown in Figure 2. The left (yellow) columns refer to the pulsed surface heating, while the right (green) columns reflect the pulsed volume one. The data are given in relative units, normalized to the contribution to the MMT values for the BaseM material, which is numerically equal to 1.13×10^7 and 3.92×10^5 for the $\gamma \ll 1$ and $\gamma \gg 1$ cases, respectively.

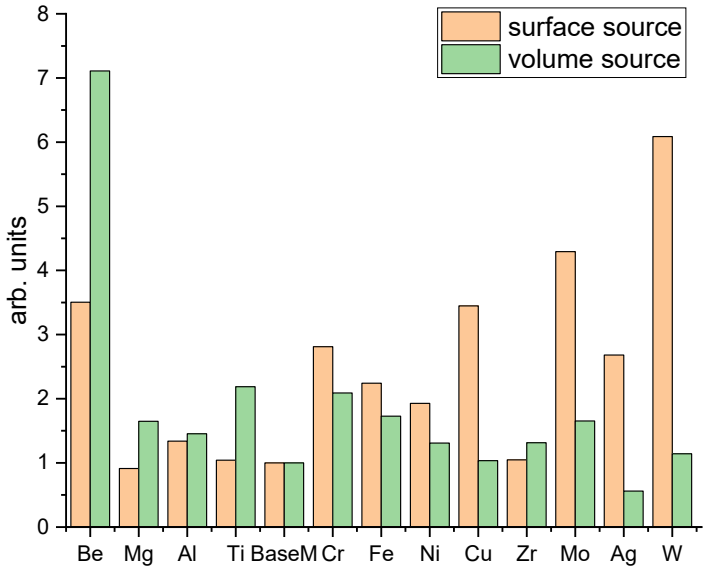

Figure 2. The contributions of the material thermophysical properties to the MMT values. Left (yellow) and right (green) columns are for the $\gamma \ll 1$ and $\gamma \gg 1$ cases, respectively.

Preprints (www.preprints.org) | NOT PEER-REVIEWED | Posted: 14 July 2023 doi:10.20944/preprints202307.0970.v1

The contributions of the material thermophysical properties into the to MMT values for the surface heating case are in a wide range: from 0.9 for the most fusible Mg in this series of materials up to 6.1 for the most refractory W. In the volume heating case, this spread is noticeably lower: from 0.6 for Ag up to 2.2 for Ti, with the exception of Be, which contribution is 7.1.

Since MMT depends on the U accelerating voltage as the $U^{\frac{3}{2}}$ power function for the $\gamma \gg 1$ case according to formula (15), it has been interesting to follow the change in both EMMT and MMT over the entire U range of the studied sources of PEBs. Figure 3 shows the calculated EMMT curves obtained using the 'HEATPACK-1.0' software package for the BaseM material at three different τ pulse durations. Also, dashed lines indicate curves calculated using analytical expressions (15) and (20) for the $\gamma \gg 1$ and $\gamma \ll 1$ cases, respectively. In addition, arrows indicate the points on the curves corresponding to certain γ values. It can be concluded that the agreement between the calculated and analytical curves is satisfactory.

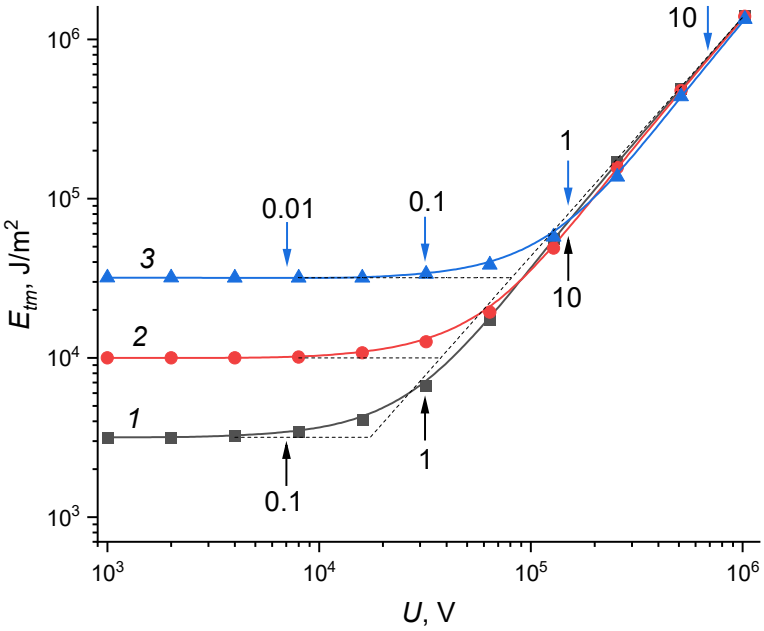

Figure 3. The EMMT versus U accelerating voltage dependences. Curves (*1*)–(*3*) for τ=0.1, 1 and 10 μs, respectively.

It follows from Figure 3 that EMMT changes by an order of magnitude as the τ pulse duration increases, from $3.2 \cdot 10^3$ J/cm^2 at τ=0.1 μs up to $3.2 \cdot 10^4$ J/cm^2 at τ=10 μs, at low U values. However, the difference between the EMMT levels decreases with increasing the U accelerating voltage, and they cease to depend on the τ pulse duration starting from a certain U value.

Figure 4 shows the calculated MMT curves for the same τ pulse durations as in Figure 3. It can be concluded from these data that the MMT behavior is completely different: the variations between its levels do not decrease, but increases with rising the U accelerating voltage. In contrast to EMMT, MMT reduces with rising the τ pulse duration.

Preprints (www.preprints.org) | NOT PEER-REVIEWED | Posted: 14 July 2023 doi:10.20944/preprints202307.0970.v1

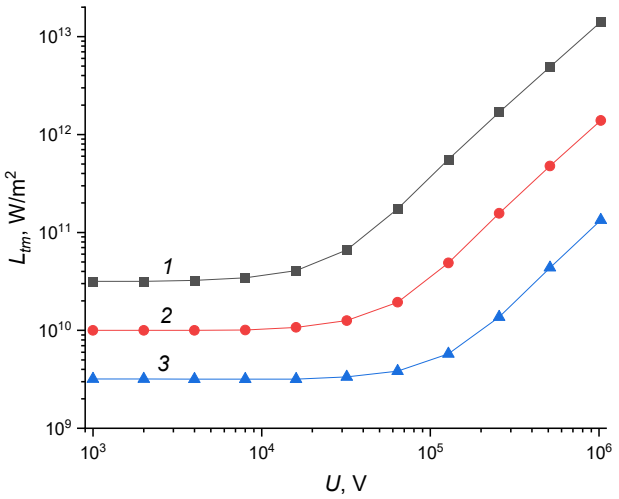

Figure 4. The MMT versus U accelerating voltage dependences. Curves (*1*)–(*3*) for τ=0.1, 1 and 10 μs, respectively.

At a given U accelerating voltage, the MMT can only be achieved by adjusting the j current density. Such $U(j)$ relationships, called current–voltage dependences (CVDs), are shown in Figure 5. They have been calculated for the same cases as presented in Figs. 3 and 4. The left branch of the CVDs is decreasing, i.e., increasing the U accelerating voltage we should reduce the j current density. The reason is that at $\gamma \ll 1$, the L_{tm} values do not depend on the U accelerating voltage. Respectively, the temperature field is only determined by the energy density of the surface source. To keep the energy input constant as the U accelerating voltage is increased (Figure 4), the j current density should be proportionally reduced. The right branch of the CVDs is increasing, i.e., when enhancing the U accelerating voltage, the j current density should also be risen. This is explained by the fact that an increase in the U accelerating voltage enhances the electron range and the heated layer thickness at $\gamma \gg 1$. It follows from formula (15) that the j current density should increase as $\sqrt{U}$ with rising the U accelerating voltage. Therefore, the inclination angle of the left branch of the CVDs is greater than that of the right one. Tracing the relationship between the CVD behavior and the γ values, it turns out that $\partial \mathrm{j} / \partial U = 0$ for γ=1.

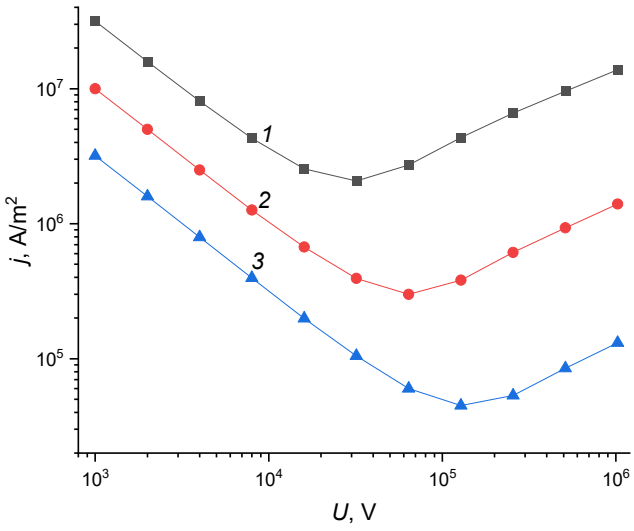

Figure 5. The current–voltage dependences for τ=0.1 (1), 1.0 (2) and 10.0 μs (3).

Preprints (www.preprints.org) | NOT PEER-REVIEWED | Posted: 14 July 2023 doi:10.20944/preprints202307.0970.v1

5. Discussion

In this section, the authors discuss in more detail some of the interesting results presented above. For example, formula (20) has been obtained from the solution of the heat equation, which determines MMT for the surface heating case ($\gamma \ll 1$). Such a formula can be written without solving differential equations, but from a simple energy balance condition. For this purpose, the Q amount of heat necessary for melting a layer with the x thickness should be assessed:

$$Q = \rho s x c (T_m - T_0), \tag{23}$$

where $s<D$ is the heated sample face area.

Dividing the left and right parts by s and substituting in (23) the estimate for the $x=0.5r_{th}$ heated layer thickness, where r_{th} is determined by formula (21), the MMT dependence can be written as:

$$L = (T_m - T_0)\sqrt{\lambda \rho c / \tau}. \tag{24}$$

Since the assumption that the entire layer of the x thickness is heated to the melting temperature is taken into account, formula (24) gives the upper MMT estimation. As for formula (20), it reflects real MMT values, considering that a temperature distribution inside the heated layer of the x thickness is non-uniform. The heated surface actually reaches the melting point, however, temperature reduces with increasing depth and is lower at the x coordinate. The difference between the exact and approximate formulas, as can be concluded from their comparison, does not depend on either the parameters of PEBs or the material properties. Approximate formula (24) always overestimates by ≈11%. This fact indicates that the layer of the x thickness is actually heated up to high temperatures close to the melting point by the end of a pulse. In addition, thermal heating turns out to be strongly localized near the surface, since the temperature drops sharply with rising depth and it is already an order of magnitude lower than the melting point at a depth of $2x$.

Discussing in more detail Figure 1, it should be noted that the 'BF–MF' phase space regions can be used for a simplified classification of PEBs. Indeed, PEBs falling into one or another region of the phase space makes it possible to draw conclusions not only about the possibility of using certain approaches to calculate temperature fields in targets, but also about their potential applications. Thus, PEBs that fall into the surface heating region are mainly applied to modify metallic surfaces and form surface alloys. Accordingly, they are not suitable for sterilizing medical materials. On the contrary, PEBs from the volume heating region cannot be used for surface modification, since they are factually suitable for sterilization of liquids, fracture of solids or microwave generation. Ones from the mixed heating region, depending on another parameter, namely the j current density, can be used in a large number of applications, such as surface modification, initiation of radiation-chemical transformations, and disinfection of biological materials.

Thereby, the 'BF–MF' phase space regions, drawn on the basis of the γ heating type criterion, enable to understand not only the nature of the thermal processes occurring under irradiation of a particular target, but also the possibility of using PEBs for certain applications. The γ heating type criterion is called complex because it depends not only on the parameters of PEBs, but also on the target material.

The contributions of the material thermophysical properties to MMT have already been considered above (Figure 2), but this parameter is more interesting as a whole, taking into account the parameters of PEBs also. In the surface heating case ($\gamma \ll 1$), MMT is described by formula (20). This expression, in addition to the term in square brackets, which reflects the contribution from the material thermophysical properties, includes the $2ierfc(0) = 1.13$ constant and the contribution from the parameters of PEBs, which is defined as the τ pulse duration with a power of –1/2. Assuming $\tau=10^{-6}$ s, we can see that MMT is equal to the contribution of the material thermophysical properties in relative units (according to Figure 2), multiplied by 10^{10} W/m^2. For Mg and W, $L_{tm} = 9.0 \cdot 10^9$ and $6.1 \cdot 10^{10}$ W/m^2, respectively. Considering formula (1), EMMT can be easy assessed for each metal also. In the surface heating case at $\gamma \ll 1$ and the τ pulse duration of 10^{-6} s, EMMT is appear to equal to the contribution of the material thermophysical properties, i.e., the height of the left (yellow)

Preprints (www.preprints.org) | NOT PEER-REVIEWED | Posted: 14 July 2023 doi:10.20944/preprints202307.0970.v1

columns in Figure 2. So, from the diagram we can easy see, for instance, that $E_{tm} = 0.9$ and 6.1 J/cm^2 for Mg and W, respectively.

For the $\gamma \gg 1$ case, the contribution to MMT from the parameters of PEBs is determined not only by the τ pulse duration, but also by the U accelerating voltage according to formula (15). Therefore, it is easier to consider an equation for EMMT, since, taking into account formula (1), expression (15) can be rewritten in a convenient way without the dependence on the τ pulse duration:

$$E_{tm} = \frac{C_0 U^{\frac{3}{2}}}{f(0)} C(T_m - T_0). \quad (25)$$

In expression (25), $f(0)$=0.9 [34]. The contribution from the parameters of PEBs is defined as the U accelerating voltage with a power of 3/2. At U=10^6 V, the contribution of the parameters of PEBs to EMMT, multiplied by the $C_0 f(0) = 1.1 \cdot 10^{-17/2}$ constant, is 3.5, and EMMT is 1.372·10^6 J/m^2 for the BaseM material. For assessing EMMT for another metal, this value should be multiplied by the contribution from the material thermophysical properties, i.e., the height of the corresponding right (green) column in Figure 2. At U=10^6 V, EMMT lie in the range (0.77–9.74)·10^6 J/m^2 for all metals, i.e., varies by an order of magnitude. When the U accelerating voltage changes by 10 times, EMMT varies proportionally by $\sqrt{1000} \approx 31.6$ times.

So, EMMT values have been considered for different materials as a function of the U accelerating voltage. For calculating MMT, formula (1) should be used, and the obtained EMMT values should be divided by the τ pulse duration.

Figure 2 is useful in that it demonstrates the different behavior of MMT for both surface and volume heating types. For surface heating, the most refractory of the considered materials are W, Mo, and Be, but Be, Ti, and Mg are those in the volume case. The latter two are simultaneously the most fusible ones in surface heating. *The behaviors of the most refractory W and the most fusible Mg are especially impressive*. Indeed, a 6.8 times higher energy density is needed for melting W in surface heating. However, the situation changes radically in volume heating. PPM of Mg is almost 1.5 times higher than that of W. This is explained by the fact that the heat capacity of the first is almost 5.5 times higher than that of the second, but during volume heating, it is the heat capacity that makes the key contribution to the MMT from thermophysical properties of materials. Figure 2 also shows that *Be is the key material for the pulsed power technologies*, which ranks third and first in terms of refractoriness for the surface and volume heating types, respectively. In pulsed volume heating MMT for Be is 3.2 times higher than that for Ti, which occupies the second place.

To facilitate the materials selection for the design of one or another component of the operating electron-beam equipment, which are simultaneously subjected to both surface and volume heating, it can be proposed to form a general series of refractoriness of metals in pulsed heating by multiplying EMMT (for both $\gamma \ll 1$ and $\gamma \gg 1$ cases). The obtained results are shown in Figure 6. The series classifies metals not only from the point of view of the complexity of the heating of surface layer up to the melting point, but also by their ability to accumulate heat upon processing. So, Be can absorb a relatively large amount of heat while remaining at a rather low temperature. Its closest competitors are Mo, W, and Cr, which are significantly (by 3.5–4.2 times) inferior in this respect.

Preprints (www.preprints.org) | NOT PEER-REVIEWED | Posted: 14 July 2023 doi:10.20944/preprints202307.0970.v1

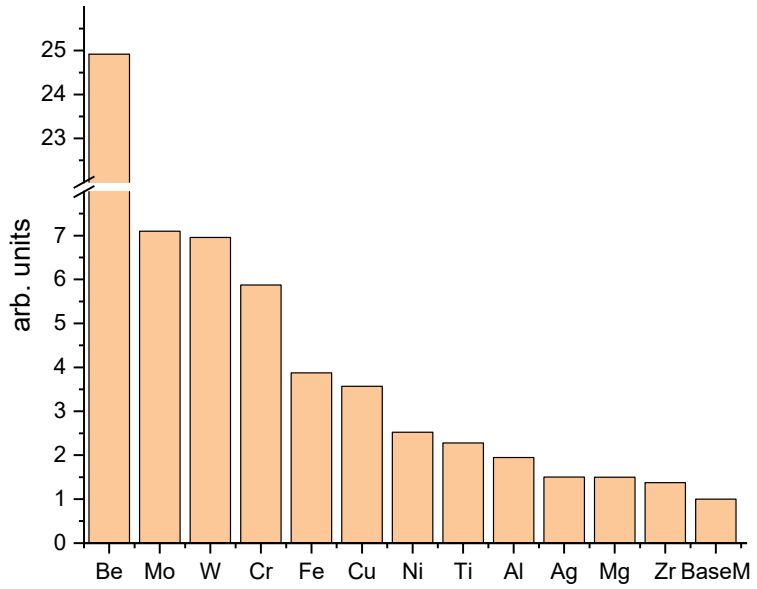

Figure 6. The refractoriness series of the metals in pulsed heating.

Figure 3 shows the changes in the EMMT behavior on the τ pulse duration with the increase in the U accelerating voltage. Based on formulas (1) and (20), EMMT has been written for the surface heating case:

$$E_{tm} = j_m U = [\sqrt{\rho c \lambda}(T_m - T_0)]\sqrt{\tau}(2ierfc(0))^{-1}. \quad (26)$$

At low U values, EMMT is described by formula (26), but by expression (25) at high U levels. It is clear why at low voltages, i.e., at $\gamma \ll 1$, with increasing pulse duration, the EMMT increases. The longer pulses, the more energy can propagate deep into the bulk and the more it needs to be delivered to the near-surface layer to compensate for heat removal. At high U, when the $\gamma \gg 1$ condition is satisfied, heat conduction is excluded from the energy propagation mechanisms, therefore, all the energy released into the surface layer remains there, and heat removal into the bulk does not occur. Accordingly, only the fact of the energy accumulation becomes important, regardless of the τ pulse duration. It is possible to input either large amount of energy upon short period of time or small amount of energy upon large period of time (see Figure 4).

Moreover, Figure 3 presents a good algorithm for satisfactorily estimating EMMT for both any materials and any PEBs. It suffices, using analytical formulas (26) and (25), to draw two straight lines, which, as we can see, describe EMMT well in all ranges, except for the $\gamma \in [0.1;1]$ interval. As for this interval, EMMT can be predicted by any known interpolation method.

Returning again to the current–voltage dependences shown in Figure 5. we should note the following. It is surprising that some conclusions can be drawn about the nature of the occurring thermal processes only by changing the parameters of PEBs and observing the target surface without any data on its thermophysical properties. Namely, when the left side of CVDs deviates from direct proportionality, the heat source ceases to be surface and becomes mixed. However, the heat source should be considered volume, when CVD passes through the the $\partial j / \partial U = 0$ point, in accordance with Figure 3. In essence, CVDs can be seen as a practical guideline for operators of various sources of PEBs to determine j current densities that provide MMT at a given U accelerating voltage.

In this study, all the above results concerning surface heat sources are true not only for PEBs, but also for other pulsed beams (laser, ion and plasma), if their parameters satisfy the $\gamma \ll 1$ condition [38–40]. However, expression (22) is not applicable in such cases, since the particle range is expressed not by formula (10), but by another one corresponding to their types.

 doi:10.20944/preprints202307.0970.v1

6. Conclusions

1. Based on the proposed complex γ heating type criterion, PEBs have been ranked for better understanding both the nature of the thermal processes occurring under irradiation and for predicting their suitability for certain applications. The γ heating type criterion is called complex because it depends not only on the parameters of PEBs, but also on the target material.
2. It has been shown that the most refractory of the considered materials are W, Mo, Be and Be, Ti, Mg in the case of pulsed surface and volume heating, respectively. However, Ti and Mg are simultaneously the most fusible ones in pulsed surface heating.
3. Both MMT and EMMT have been calculated over the wide ranges of U accelerating voltages and τ pulse durations. At low U levels ($\gamma \ll 1$), EMMT increases with rising the τ pulse duration. The longer the τ pulse duration, the more energy is transmitted into a target bulk and the more it needs to be input to the surface layer. At high U levels ($\gamma \gg 1$), heat removal into the target bulk does not occur. Therefore, only the fact of accumulation of a given amount of energy becomes important, regardless of the τ pulse duration.
4. It was established that to calculate MMT and EMMT for any both materials and PEBs, it is sufficient to use analytical formulas (26) and (25) and interpolate the data within the $\gamma \in [0.1;1]$ interval.
5. The general refractoriness series of metals is ranked for pulsed heating processes. It classifies metals not only in terms of the complexity of their heating up to the melting points, but also by their ability to accumulate heat under irradiation.
6. Be is the unique refractory material in pulsed heating processes. It can absorb a relatively large amount of heat without a noticeable rise in temperature. The closest ones are Mo, W, and Cr, which are significantly (by 3.5–4.2 times) inferior in this respect.
7. The temperature distribution profile in a target under irradiation with PEBs, normalized to the electron range, does not depend on the density of the target material in the case of a volume heat source. The reason is the mutual compensation of two opposite tendencies. On the one hand, the specific density of nuclei increases in direct proportion to the substance density, and temperature should reduce at a fixed energy. On the other hand, the energy release volume decreases due to the inversely proportional relationship between the electron range and the substance density, and temperature should increase.
8. The CVDs have been calculated, which can be considered as practical guidelines for determining the j current densities that provide MMT at a given U accelerating voltage.
9. Some conclusions can be drawn about the nature of the occurring thermal processes inside the target, observing only the CVD behavior, without any data on material thermophysical properties. Namely, when the left side of CVDs deviates from direct proportionality, the heat source ceases to be surface and becomes mixed. Moreover, the heat source can be considered volume, when it passes through the $\partial j/\partial U=0$ point.

Author Contributions: Conceptualization, methodology, investigation, writing, A.M.

Funding: Analysis of the sources of pulsed electron beams and their classification was made with the support by the Ministry of Science and Higher Education of the Russian Federation (project No FWRF-2021-0001). Whereas analysis of materials behavior at pulsed heating the was made with the support by the Ministry of Science and Higher Education of the Russian Federation (project No. 075-15-2021-1348).

Acknowledgments**:** The author is grateful to Dr. Mikhail Slobodyan for fruitful discussions

Conflicts of Interest: The authors declare no conflict of interest.

References

1. Koval', N.N.; Ivanov, Y.F. Nanostructuring of surfaces of metalloceramic and ceramic materials by electron-beams. *Russian Physics Journal* **2008,** 51, 505–516. https://doi.org/10.1007/s11182-008-9073-7
2. Koval, N.N.; Koval, T.V.; Krysina, O.V.; Ivanov, Y.F.; Teresov, A.D.; Moskvin, P.V.; Tran, M.K.A.; Prokopenko, N.A.; Petrikova, E.A. Experimental Study and Mathematical Modeling of the Processes

Occurring in ZrN Coating/Silumin Substrate Systems under Pulsed Electron Beam Irradiation. *Coatings* **2021**, 11, 1461. https://doi.org/10.3390/coatings11121461

3. Krysina, O.V.; Teresov, A.D.; Moskvin, P.V.; Koval, N.N.; Ivanov, Yu. F.; Akhmadeev, Yu. H.; Lopatin I. V. Variation in the Local Material Temperature During Electron Beam Treatment and its Influence on the Modified Layer Properties. *Russian Physics Journal* **2019,** 62, 1139–1146. https://doi.org/10.1007/s11182-019-01828-3
4. Geng, Y.; Chen, X.; Konovalov, S.; Panchenko, I.; Ivanov, Yu.; Deev, V.; Prusov, E. Ultrafast microstructure modification by pulsed electron beam to enhance surface performance. *Surface and Coatings Technology* **2022**, 434, 128226, https://doi.org/10.1016/j.surfcoat.2022.128226.
5. Gromov, V.E.; Konovalov, S.V.; Ivanov, Yu.F.; Shliarova, Yu.A.; Vorobyov, S.V.; Semin, A.P. Structure and properties of the CrMnFeCoNi high-entropy alloy irradiated with a pulsed electron beam. *Journal of Materials Research and Technology* **2022**, 19, 4258-4269, https://doi.org/10.1016/j.jmrt.2022.06.108.
6. Ozur, G.E.; Proskurovsky, D.I. Generation of Low-Energy High-Current Electron Beams in Plasma-Anode Electron Guns. *Plasma Phys. Rep.* **2018**, 44, 18–39. https://doi.org/10.1134/S1063780X18010130
7. Ozur, G.; Proskurovsky, D.; Rotshyein, V.; Markov, A. Production and application of low-energy, high-current electron beams. *Laser and Particle Beams* **2003**, 21(2), 157-174. doi:10.1017/S0263034603212040
8. Markov, A.; Yakovlev, E.; Petrov, V. Formation of Surface Alloys With a Low-Energy High-Current Electron Beam for Improving High-Voltage Hold-Off of Copper Electrodes. *IEEE Transactions on Plasma Science* **2013,** 41, 2177-2182. DOI:10.1109/TPS.2013.2254501
9. Dong, C,; Wu, A.; Hao, S.; Zou, J.; Liu, Z.; Zhong P.; Zhang A.; Xu T.; Chen, J.; Xu, J.; Liu Q.; Zhou, Z. Surface treatment by high current pulsed electron beam. *Surface and Coatings Technology* **2003**, 163–164, 620-624, https://doi.org/10.1016/S0257-8972(02)00657-6.
10. Liu, S.; Fu J.; Shen X.; Chen B.; Han, X. Improved wear resistance of cemented carbide impact needle under high frequency micro-amplitude impact treated by high current pulsed electron beam, *Wear* 2023, 518–519, 204632. https://doi.org/10.1016/j.wear.2023.204632.
11. Tian N.; Guan, J.; Zhang, C.; Lyu, P.; Peng, C.; Cai, J.; Guan, Q. Influence of high-current pulsed electron beam irradiation on element diffusion behavior and mechanical properties of TC4/304 stainless steel diffusion bonded joints, *Materials Characterization* **2023**, 198, 112713. https://doi.org/10.1016/j.matchar.2023.112713.
12. Lu, J.; Sui, X.; Yang, B.; Chen, J.; Cai, L.; Zhou, S.; Li, W.; Jiang, M.; Hao, S. Ultrafast in-situ transformation of graphite into graphene nanosheets by high current pulsed electron beam direct irradiation. *Applied Surface Science* **2022**, 572, 151498. https://doi.org/10.1016/j.apsusc.2021.151498.
13. Fedorov, S. V.; Kozochkin, M.; Stebulyanin, M. Control of the surface electron-beam alloying process by vibration monitoring Sergey. *Mechanics & Industry* **2018**, 19, 702. DOI: https://doi.org/10.1051/meca/2018050
14. Fedorov, S.V.; Pavlov, M.D.; Okunkova, A.A. Effect of structural and phase transformations in alloyed subsurface layer of hard-alloy tools on their wear resistance during cutting of high-temperature alloys. *J. Frict. Wear* **2013,** 34, 190–198. https://doi.org/10.3103/S1068366613030069
15. Fedorov, S.V.; Aleshin, S.V.; Swe, M.H.; Abdirova, R.; Kapitanov, A.; Egorov, S. Comprehensive surface treatment of high-speed steel tool. *Mechanics & Industry* **2017**, 18, 711. DOI:10.1051/MECA/2017066
16. Meisner, S.N.; Vlasov, I.V.; Yakovlev, E.V.; Panin, S.V.; Meisner, L.L.; D'yachenko, F.A. Impact of electron beam surface modification on deformation behavior and fracture properties of TiNi shape memory alloy. *Materials Science and Engineering: A* **2019**, 740–741, 381-389. https://doi.org/10.1016/j.msea.2018.10.113.
17. Morini, F.; Bestetti, M,; Franz, S.; Vicenzo, A.; Markov, A.; Yakovlev, E. Surface properties modification of magnesium alloys by low energy high current pulsed electron beam. *Surface and Coatings Technology* **2021**, 420, 127351. https://doi.org/10.1016/j.surfcoat.2021.127351.
18. Yakovlev, E.; Pesterev, E.; Petrov, V.; Maznoy, A. Preparation of Al-Dy core-shell particles by electron beam treatment of Al powder with consequent magnetron deposition of Dy film. *Materials Letters* **2022**, 324, 132729. https://doi.org/10.1016/j.matlet.2022.132729.
19. Murray, J.W.; Kinnell, P.K.; Cannon, A.H.; Bailey, B.; Clare, A.T. Surface finishing of intricate metal mould structures by large-area electron beam irradiation. *Precision Engineering* **2013**, 37, 443-450. https://doi.org/10.1016/j.precisioneng.2012.11.007.
20. Tokunaga, J.; Kojima, T.; Kinuta, S.; Wakabayashi, K.; Nakamura, T.; Yatani, H.; Sohmura, T. Large-area electron beam irradiation for surface polishing of cast titanium. *Dental Materials Journal* **2009**, 28, 571-577. https://doi.org/10.4012/dmj.28.571
21. Engelko, V.; Yatsenko, B.; Mueller, G.; Bluhm, H. Pulsed electron beam facility (GESA) for surface treatment of materials. *Vacuum* **2001**, 62, 211-216. https://doi.org/10.1016/S0042-207X(00)00446-2.
22. Fetzer, R.; An, W.; Weisenburger, A.; Mueller, G. Pulsed electron beam facility GESA-SOFIE for in-situ characterization of cathode plasma dynamics, *Vacuum* **2017**, 145, 179-185. https://doi.org/10.1016/j.vacuum.2017.08.038.

23. Astrelin, V.T.; Kandaurov, I.V.; Vorobyov, M.S.; Koval, N.N.; Kurkuchekov, V.V. ; Sulakshin, S.A.; Trunev, Yu A. Generation and transport of submillisecond intense electron beams in plasma cathode vacuum diodes. *Vacuum* **2017**, 143, 495-500. https://doi.org/10.1016/j.vacuum.2017.03.025.
24. Vorobyov, M. S.; Koval, N. N.; Sulakshin S. A. An electron source with a multiaperture plasma emitter and beam extraction into the atmosphere. *Instruments and Experimental Techniques 2015*, 58, 687–695. DOI: 10.1134/S0020441215040132
25. Koval, N. N.; Devyatkov, V. N.; Vorobyev, M. S. Electron sources with plasma grid emitters: progress and prospects. *Russian Physics Journal* **2021**, 63, 1651-1660. DOI: 10.1007/s11182-021-02219-3
26. Remnev, G E.; Furman, E G.; Pushkarev, A I.; Karpuzov, S B.; Kondrat'ev, N. A.; Goncharov, D. V. A High-Current Pulsed Accelerator with a Matching Transformer. *Instruments and Experimental Techniques* **2004**, 47, 394–398. https://doi.org/10.1023/B:INET.0000032909.92515.b7
27. Pushkarev, A.I.; Novoselov, Y.N.; Sazonov, R.V. Losses in a pulsed electron beam during its formation and extraction from the diode chamber of an accelerator. *Instruments and Experimental Techniques* **2007**, 50, 687–694. https://doi.org/10.1134/S0020441207050089
28. Pushkarev, A.; Prima, A.; Ezhov, V.; Miloichikova, I.; E. Petrenko. Determination of the Pulsed Electron Beam Spectrum by Current and Voltage Oscillograms". *Laser and Particle Beams* **2021**, 8815697. https://doi.org/10.1155/2021/8815697
29. Korovin, S.D.; Rostov, V.V. High-current nanosecond pulse-periodic electron accelerators utilizing a tesla transformer. *Russian Physics Journal* **1996**, 39, 1177–1185. https://doi.org/10.1007/BF02436160
30. Kim, A.A.; Kovalchuk, B.M.; Kokshenev, V.A.; Shishlov, A.V.; Ratakhin, N.A.; Oreshkin, V.I.; Rostov, V.V.; Koshelev, V.I.; Losev, V.F. Review of high-power pulsed systems at the Institute of High Current Electronics. *Matter and Radiation at Extremes* **2016**, 1, 201-206. https://doi.org/10.1016/j.mre.2016.08.001.
31. Gnyusov, S.F.; Rotshtein, V.P.; Mayer, A.E.; Astafurova, E.G.; Rostov, V.V.; Gunin A.V.; Maier, G.G. Comparative study of shock-wave hardening and substructure evolution of 304L and Hadfield steels irradiated with a nanosecond relativistic high-current electron beam. *Journal of Alloys and Compounds* **2017**, 714, 232-244. https://doi.org/10.1016/j.jallcom.2017.04.219.
32. Markov, A.B.; Kitsanov, S.A.; Rotshtein, V.P.; Polenin, S. D.; Proskurovskii, D. I.; Dudarev E. F. Dynamic fracture of copper under the action of a relativistic high-current electron beam. *Russian Physics Journal* **2006**, 49, 758–765. https://doi.org/10.1007/s11182-006-0172-z
33. Yushkov, Y.G.; Oks, E.M.; Tyunkov, A.V.; Zolotukhin, D.B. Electron-Beam Synthesis of Dielectric Coatings Using Forevacuum Plasma Electron Sources (Review). *Coatings* **2022**, 12, 82. https://doi.org/10.3390/coatings12010082
34. Rotshtein, V.; Ivanov, Yu.; Markov, A. Chapter 6 Surface Treatment of Materials with Low-Energy, High-Current Electron Beams. In *Materials Surface Processing by Directed Energy Techniques;* Pauleau, Y., Ed; Elsevier, 2006, pp. 205-240. https://doi.org/10.1016/B978-008044496-3/50007-1.
35. Markov A.B.; Rotshtein, V.P. Calculation and experimental determination of dimensions of hardening and tempering zones in quenched U7A steel irradiated with a pulsed electron beam. *Nuclear Instruments and Methods in Physics Research Section B: Beam Interactions with Materials and Atoms* **1997**, 132, 79-86. https://doi.org/10.1016/S0168-583X(97)00416-3.
36. Handbook of physical properties, Gigorjev, I.S.; Meilikhov E.Z.; Ed; Energoatomizdat, Moscow, 1991.
37. Meisner, L.L.; Markov, A.B.; Proskurovsky, D.I.; Rotshtein, V.P.; Ozur, G.E.; Meisner, S.N.; Yakovlev E.V.; Poletika, T.M.; Girsova, S.L.; Semin, V.O. Effect of inclusions on cratering behavior in TiNi shape memory alloys irradiated with a low-energy, high-current electron beam. *Surface and Coatings Technology* **2016**, 302, , 495-506, https://doi.org/10.1016/j.surfcoat.2016.06.036.
38. Remnev, G.E.; Isakov, I.F.; Opekounov, M.S.; Kotlyarevsky, G.I.; Kutuzov, V.L.; Lopatin, V.S.; Matvienko, V.M.; Ovsyannikov, M.Yu.; Potyomkin, A.V.; Tarbokov, V.A. High-power ion beam sources for industrial application. *Surface and Coatings Technology* **1997**, 96, 103-109. https://doi.org/10.1016/S0257-8972(97)00116-3.
39. Remnev G.E.; Isakov I.F.; Opekounov M.S.; Matvienko, V.M.; Ryzhkov, V.A.; Struts, V.K.; Grushin, I.I.; Zakoutayev, A.N.; Potyomkin, A.V;. Tarbokov, V.A.; Pushkaryov, A.N.; Kutuzov, V.L.; Ovsyannikov, M.Yu., High intensity pulsed ion beam sources and their industrial applications. *Surface and Coatings Technology***1999**, 114, 206-212. https://doi.org/10.1016/S0257-8972(99)00058-4.
40. Xu, M.; Yu, X.; Zhang, S.; Yan, S.; Tarbokov, V.; Remnev G.; Le X. Microstructure Formation and Mechanical Properties of Metastable Titanium-Based Gradient Coating Fabricated via Intense Pulse Ion Beam Melt Mixing. *Materials* **2023**, 16(8), 3028; https://doi.org/10.3390/ma16083028 - 11 Apr 2023